Steel and Composite Structures, *Vol. 18, No. 5 (2015) 1177-1195*
DOI: http://dx.doi.org/10.12989/scs.2015.18.5.1177

Cyclic test for beam-to-column abnormal joints in steel moment-resisting frames

Zu Q. Liu [*1], Jian Y. Xue [1], Xiu N. Peng [2] and Liang Gao [1]

[1] *College of Civil Engineering, Xi'an University of Architecture and Technology, Xi'an, China*
[2] *College of Civil and Architectural Engineering, Guangxi University, Nanning, China*

(*Received April 25, 2014, Revised September 29, 2014, Accepted November 10, 2014*)

Abstract. Six specimens are tested to investigate the cyclic behavior of beam-to-column abnormal joints in steel moment-resisting frames, which are designed according to the principle of strong-member and weak-panel zone. Key parameters include the axial compression ratio of column and the section depth ratio of beams. Experimental results indicate that four types of failure patterns occurred during the loading process. The P-Δ hysteretic loops are stable and plentiful, but have different changing tendency at the positive and negative direction in the later of loading process due to mechanical behaviors of specimens. The ultimate strength tends to increase with the decrease of the section depth ratio of beams, but it is not apparent relationship to the axial compression ratio of column, which is less than 0.5. The top panel zone has good deformation capacity and the shear rotation can reach to 0.04 rad. The top panel zone and the bottom panel zone don't work as a whole. Based on the experimental results, the equation for shear strength of the abnormal joint panel zone is established by considering the restriction of the bottom panel zone to the top panel zone, which is suitable for the abnormal joint of H-shaped or box column and beams with different depths.

Keywords: cyclic loading; beam-to-column abnormal joint; shear strength; hysteretic performance; mechanical behavior

1. Introduction

Beam-to-column joint is a main component in the steel moment-resisting frame, which has a direct influence on the stability of structure (Yang and Kim 2007, He *et al.* 2010, Loulelis *et al.* 2012, Lee *et al.* 2013). According to the difference of configurations, beam-to-column joint can be divided into normal joint and abnormal joint (Fig. 1). Abnormal joint is defined as the joint of beams with different section depths and (or) columns with different section depths (Peng 2010). Due to the increase of load and the special requirement of structure layout, abnormal joint has been widely used in the steel moment-resisting frame. The behavior of abnormal joint is also studied using experimental investigation and theoretical analysis by some researchers: Imai *et al.* (1991) tested abnormal joints of H-shaped column and H-shaped beams with different depth under the monotonic loading, and the evaluation equation for strength was established by introducing

*Corresponding author, Ph.D., E-mail: liuzuqiang0081@126.com

http://www.techno-press.org/?journal=scs&subpage=8 ISSN: 1229-9367 (Print), 1598-6233 (Online)

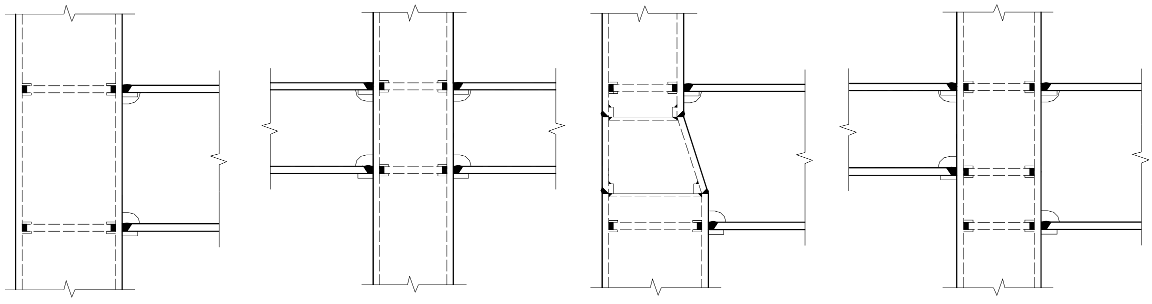

(a) Normal joint (b) Abnormal joint

Fig. 1 Beam-to-column joints in steel moment-resisting frames

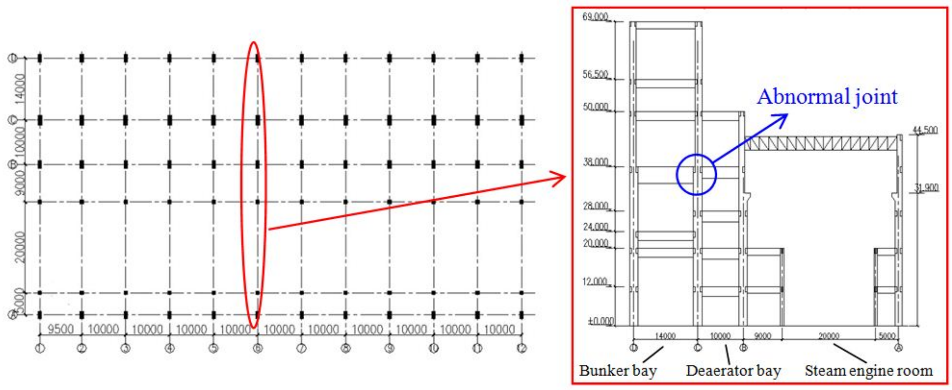

Fig. 2 Steel moment-resisting frame in thermal power plant

appropriate parameters. Kuwahara *et al*. (2000) presented theoretical and experimental investigations on the behavior of the panel zone of abnormal joints, which were composed of box column and H-shaped beams with different depth, and the calculated equations for stiffness and strength of the panel zone were proposed. Li and Chen (2009) put forward a calculated method of shear strength for the panel zone of abnormal joint of circular hollow section column and two H-shaped beams with different depth. Sui *et al*. (2013) made a series of numerical analysis on the elasto-plastic behavior of abnormal joints of circular hollow section column and two H-shaped beams with different depth, and proposed a design method for the abnormal joint with an exterior reinforcing ring. There are many types of abnormal joints, of which the behaviors are different.

The abnormal joint of box column with H-shaped beam and box beam has been used in steel moment-resisting frame (Fig. 2) of thermal power plant, which is an establishment about electricity generation and power transformation .In spite of the extensive studies of abnormal joints in the literature, the topics on the seismic performance and design method of this type of abnormal joint have not been fully addressed. For this reason, cyclic tests on abnormal joints of box column with H-shaped beam and box beam were conducted. The failure patterns, hysteretic performance and shear deformations of the panel zone were determined, and the mechanical behaviors were revealed. Finally, the equation for shear strength of the abnormal joint panel zone was established.

2. Experimental program

2.1 Specimen descriptions

The specimens were double-side beam-to-column assemblies that are representative of interior beam-to-column joint. The dimensions and geometry of the specimens are shown in Fig. 3. With the difference of the section depth of beams, the panel zone is divided into two parts, which are named as the top panel zone and the bottom panel zone in this paper. The key parameters were the axial compression ratio of column and the section depth ratio of beams, the latter of which can be calculated by Eq. (1).

$$\beta = \frac{d_{b1}}{d_{b2}} \tag{1}$$

In which β is the section depth ratio of beams, d_{b1} and d_{b2} are the depths of beams at both sides of the abnormal joint, respectively, $d_{b1} \leq d_{b2}$.

For the fabrication of the specimens, welded-bolted connection was used between H-shaped beam and column, and welded connection was used between box beam and column. The details of specimens are shown in Fig. 4 and are summarized in Table 1.

In order to study the shear strength of the panel zone, the specimens were designed according to the principle of strong-member and weak-panel zone. The thickness of the web at the panel zone was weaken to half of that at the other parts of the column.

2.2 Material properties

All specimens were fabricated with grade Q235 steel. The material properties have been

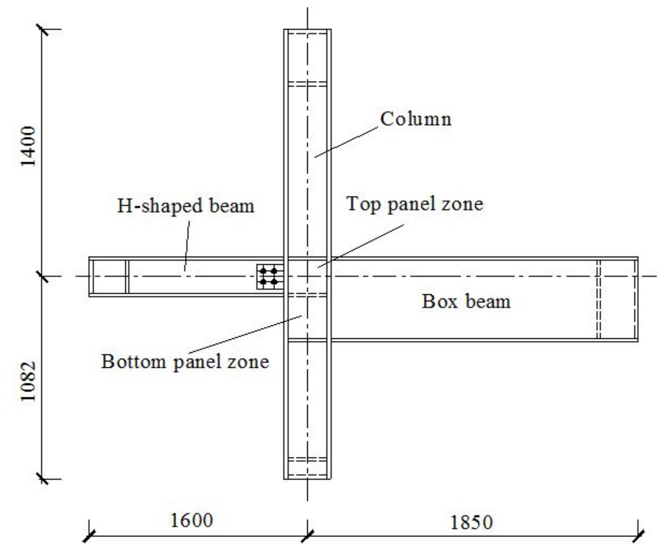

Fig. 3 Global dimensions and geometry of the specimen

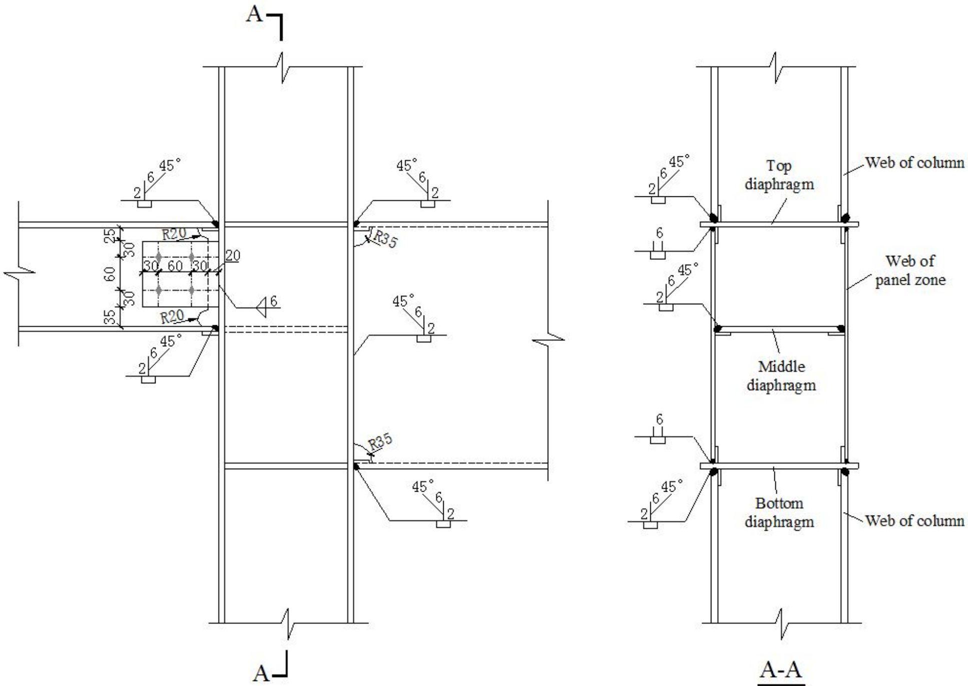

(a) Detail of specimen-JD20

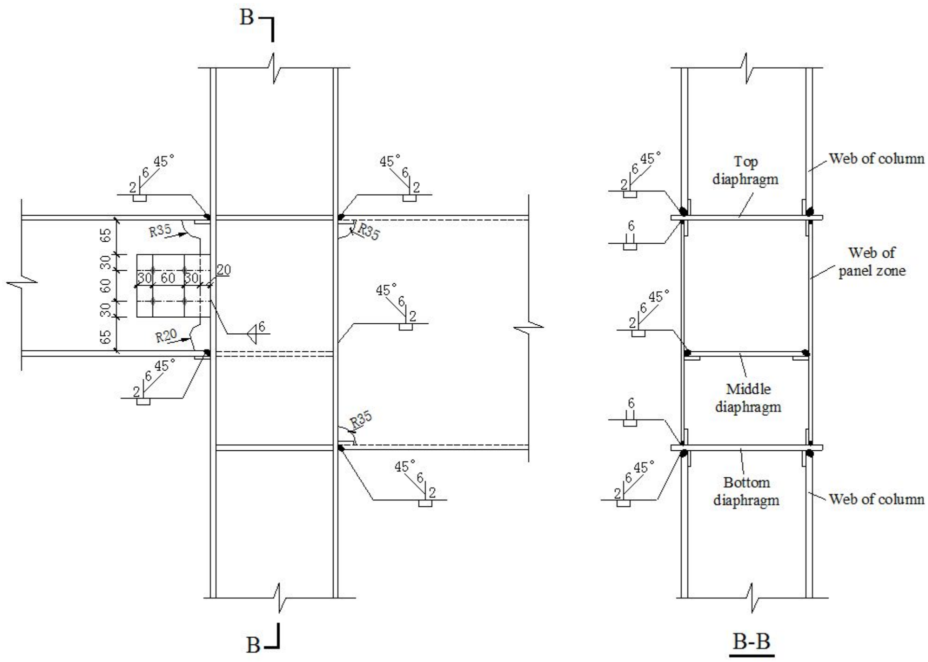

(b) Detail of specimen-JD27

Fig. 4 Details of the specimens

Table 1 Dimensions of member section and key parameters

Specimen	H-shaped beam		Box beam		Box column		Section depth ratio of beams	Axial compression ratio*
	Flange (mm)	Web (mm)	Flange (mm)	Web (mm)	Flange (mm)	Web (mm)		
JD20-1	150 × 10	180 × 10	200 × 10	430 × 10	250 × 12	226 × 12 (226 × 6)*	0.44	0.2
JD20-2	150 × 10	180 × 10	200 × 10	430 × 10	250 × 12	226 × 12 (226 × 6)	0.44	0.3
JD20-3	150 × 10	180 × 10	200 × 10	430 × 10	250 × 12	226 × 12 (226 × 6)	0.44	0.4
JD27-1	150 × 10	250 × 10	200 × 10	430 × 10	250 × 12	226 × 12 (226 × 6)	0.60	0.2
JD27-2	150 × 10	250 × 10	200 × 10	430 × 10	250 × 12	226 × 12 (226 × 6)	0.60	0.3
JD27-3	150 × 10	250 × 10	200 × 10	430 × 10	250 × 12	226 × 12 (226 × 6)	0.60	0.4

*The data in brackets corresponds with the dimension of the panel zone; axial compression ratio represents the ratio of section related to the abnormal joint panel zone.

Table 2 Experimental results of material properties

Plate thickness t/mm	Yield stress f_y/MPa	Yield strain ε_y	Tensile strength f_u/MPa	Elastic modulus E_s/MPa	Elongation δ/%
6	310.5	0.001540	453.1	2.02×10^5	37.5
10	285.7	0.001390	431.0	2.07×10^5	43.5
12	286.4	0.001392	449.3	2.07×10^5	33.1

determined by coupon tensile tests as prescribed by relevant standards. The results of the tests are summarized in Table 2.

2.3 Test setup and procedure

The basic configuration of a typical test setup and the location of instrumentations are represented in Fig. 5. It was designed in order to simulate the conditions of the abnormal joint within the frame structure. The specimens were pinned at the bottom end of column and beam ends and free at the top end of column. The axial compression load was applied to the column through a vertical jack and kept invariable during the test process, and then low cyclic reversed load was applied to the top end of column by horizontal actuator. The out-of-plane displacements of specimens were completely restricted.

The vertical actuator had a 1,500 kN capacity in compression, and the horizontal actuator had a force capacity of ± 1,000 kN and a displacement capacity of ± 350 mm. The instrumentations used in this test were the load cells, linear variable displacement transducers (LVDTs), dial gauges, and strain gauges. The load and displacement of the top end of column were measured respectively by load cell and displacement transducer, which were installed in the horizontal actuator. The load of beam ends was measured by two load cells. Measurement of the relative rotation at the panel zone was given with particular attention. Two dial gauges were set diagonally on the top panel zone and the bottom panel zone respectively to measure the shear deformation. Strain gauges were mounted to capture strains adjacent to the panel zone, column web and flange and beam web and flange, as shown in Fig. 6.

According to JGJ101-1996 (1997), the loading history for the tests was divided into two phases, as shown in Fig. 7. At the initial phase, the tests were conducted under force control. Force

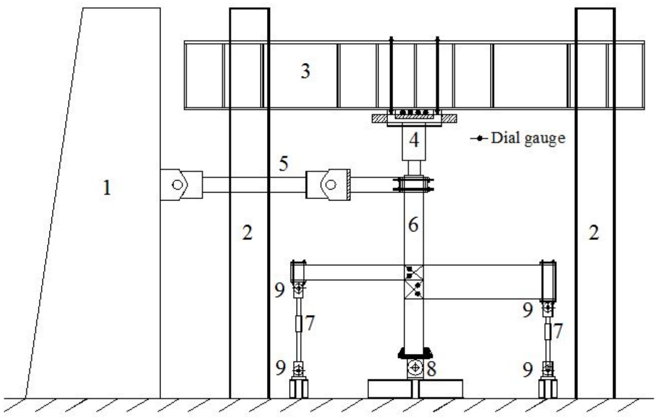

(1) Reaction wall; (2) Reaction column; (3) Reaction beam; (4) Vertical actuator; (5) Horizontal actuator
(6) Specimen; (7) Load cell; (8) Single-hinge support under column; (9) Single-hinge support at beam end

Fig. 5 Test setup

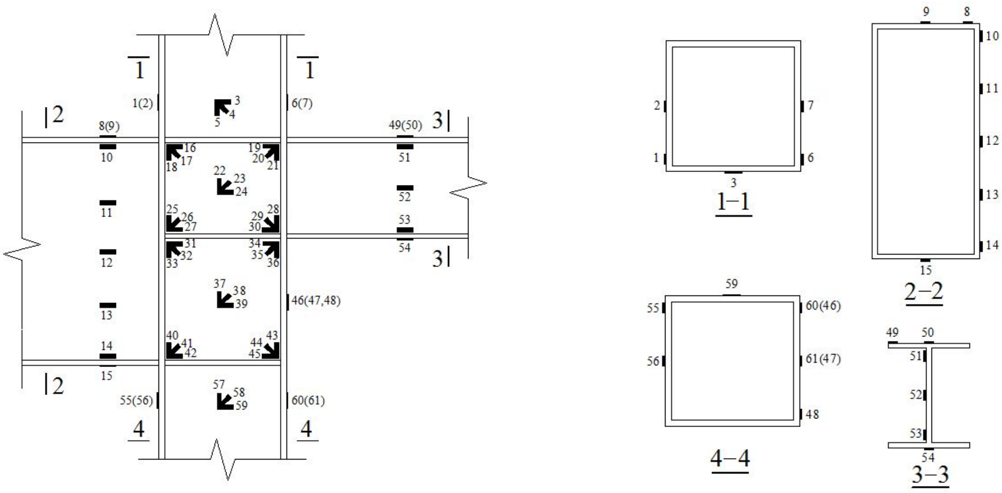

(a) (b)

Fig. 6 Strain gages

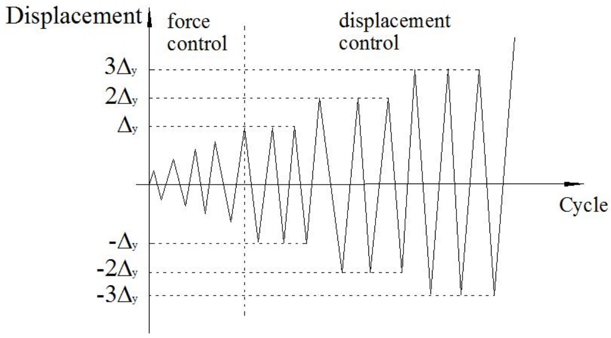

Fig. 7 Loading history

increments of 20 kN were used and every load level was circulated one cycle. When the specimens started yielding, the tests were conducted under displacement control. If the yield displacement is denoted as Δ_y, displacement increments of Δ_y were used, and three cycles were applied at every load level. This procedure was continued until failure of the specimens.

3. Experimental results

3.1 Failure process

Six specimens have the similar failure process. Because the panel zone was weaker than the members, the failure of the specimen initiated at the panel zone. It can be seen from the values measured by strain gauges that the center of the top panel zone yielded first and then the yield field expanded slowly to the surrounding area. When the top panel zone yielded completely, the bottom panel zone began to yield from the center, and then the yield field developed to surrounding. Fig. 8 shows the change trend of strains of the panel zone of JD27-1, in which P is the load applied to the top end of the column and ε is the strains measured by strain gauges.

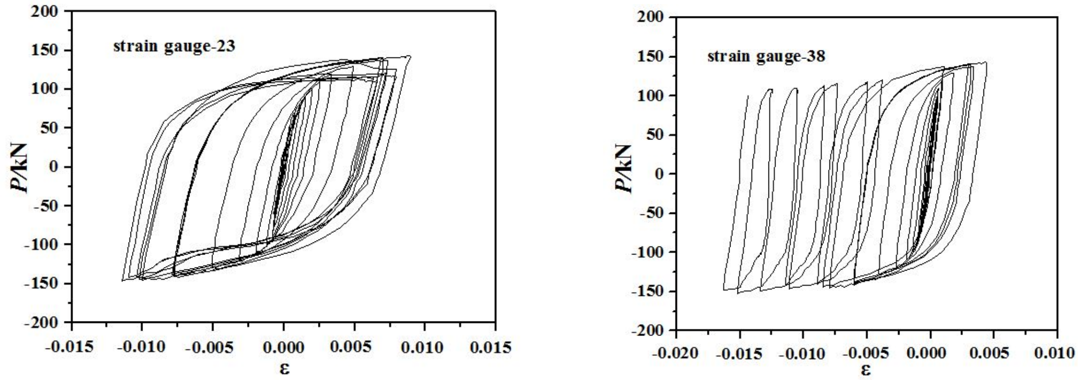

(a) Top panel zone (b) Bottom panel zoned

Fig. 8 Strain of the panel zone (JD27-1)

After the panel zone yielding, there were four types of failure patterns occurring in sequence during the following loading process: (1) weld between the box beam bottom flange and the column flange cracked (Fig. 9(a)); (2) weld between the box beam web and the column flange cracked (Fig. 9(b)); (3) weld between the bottom diaphragm and the column flange cracked, and then the crack propagated rapidly up to the weld between the bottom panel zone and the column flange and down to the weld between the column web and flange (Fig. 9(c)); (4) local buckling occurred at the top panel zone (only JD20-3, JD27-2 and JD27-3) (Fig. 9(d)).

Until the loading terminated, no yield occurred at the end of beams and columns, as shown in Fig. 10, in which *P* and *ε* are the same as Fig. 8.

Analyzing the failure process of the specimens, observations can be made as follows:

(1) The section bending-stiffness of box beam is larger than that of H-shaped beam, so the moment carried by box beam is much larger than that by H-shaped beam based on the internal force balance of the joint. As a result, the failure of weld between the box beam and the column is serious, and there is nearly no crack at the weld between the H-shaped beam and the column.

(2) There is serious stress concentration at the toe of weld between the box beam and the column, which results in the initiate of crack.

(3) Compared with the weld between the box beam top flange and the column, the weld

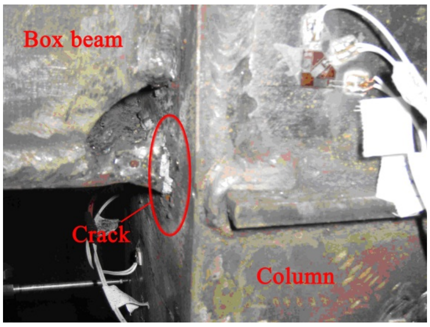

(a) Crack of weld between the box beam bottom flange and the column flange

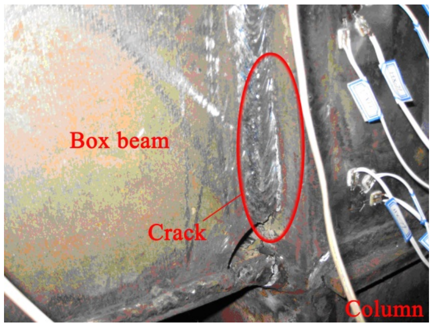

(b) Crack of weld between the box beam web and the column flange

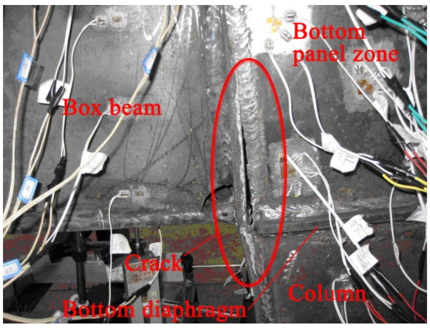

(c) Crack of weld between the bottom diaphragm and the column flange and its propagation

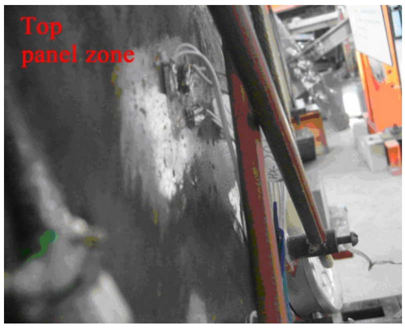

(d) Local buckling of the top panel zoned

Fig. 9 Failure patterns of specimens

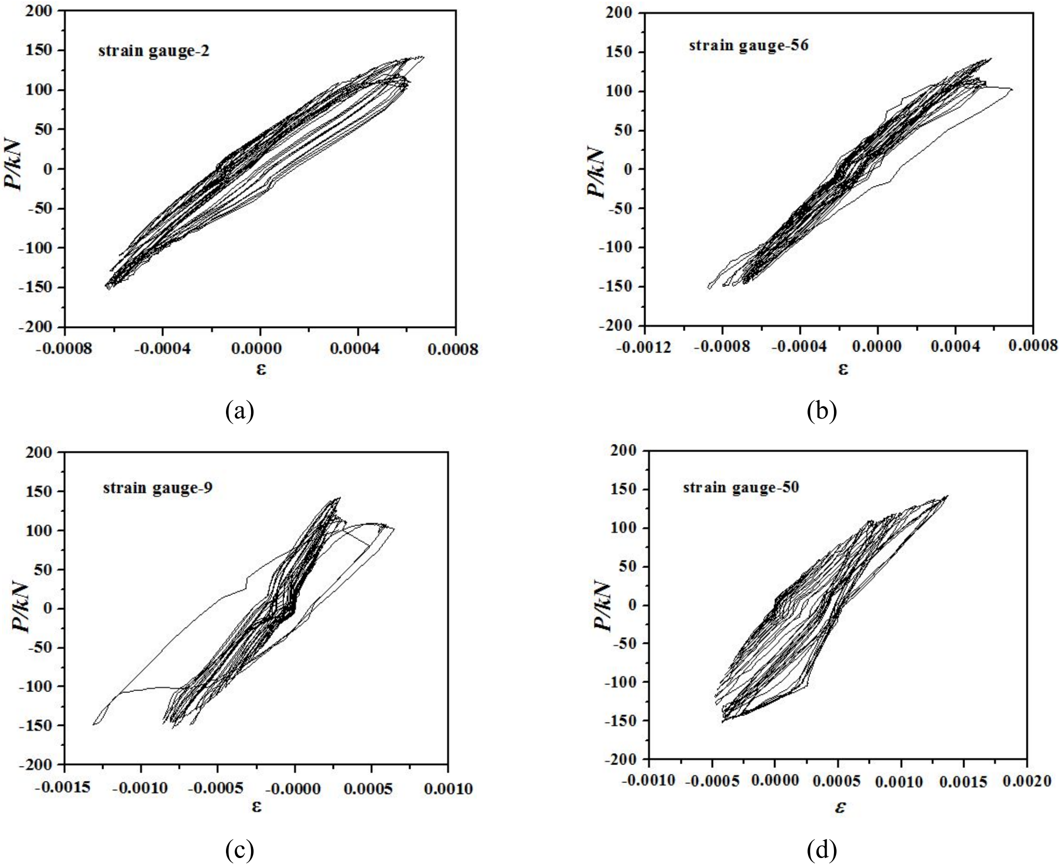

Fig. 10 Strain of the beam and column ends (JD27-1)

between the box beam bottom flange and the column failed badly. The reason is that the internal force of the box beam top flange can transfer to the H-shaped beam top flange, but that of the box beam bottom flange can only transfer to the column. Therefore, the weld between the box beam bottom flange and the column is in the worse mechanical state than that between the box beam top flange and the column.

(4) The shear deformation of the top panel zone was larger than that of the bottom panel zone, so local buckling occurred at the top panel zone rather than the bottom panel zone. For the specimens with larger axial compression ratio, such as JD20-3 and JD27-3, local buckling of the top panel zone occurred easily. The width-thickness ratio of the top panel zone of JD27-2 was larger than that of JD20-2, so local buckling occurred on the former.

3.2 P-Δ hysteretic loops

The P-Δ hysteretic loops of specimens are shown in Fig. 11, in which P is the same as Fig. 8 and Δ is the displacement at the top end of the column. The hysteretic curves are compared, and observations can be made as follows:

All the hysteretic loops of the abnormal joints are in a shuttle type, and as a result, the energy dissipated per loop is good, and all of them are stable and plentiful. However, because of the weld cracks widening suddenly, the positive load reduced rapidly. The curves at the pushed and pulled directions (as shown in Fig. 12) have different changing tendency in the later loading process, and this is closely related to mechanical behaviors of the specimens, which is discussed below.

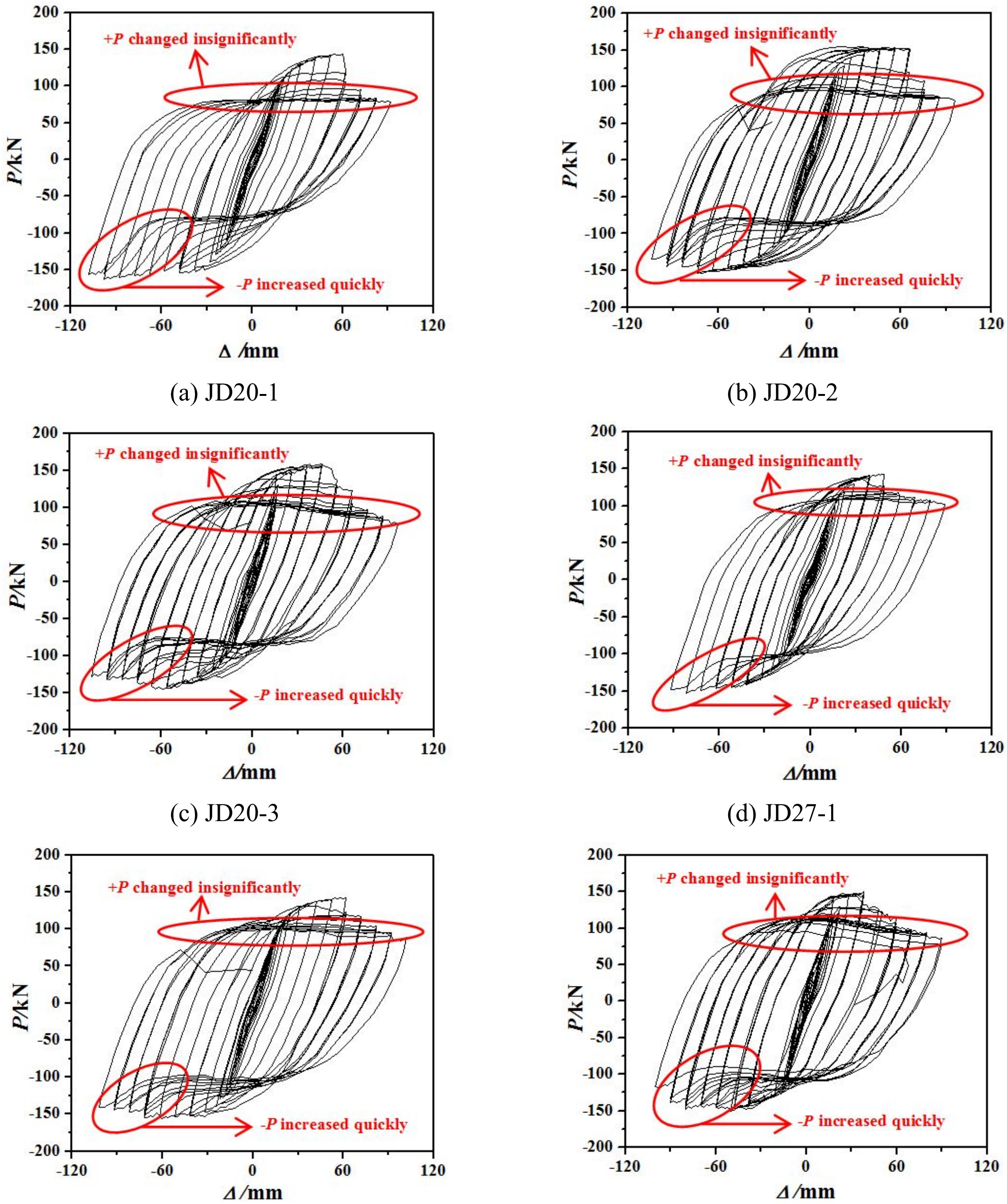

(a) JD20-1 (b) JD20-2

(c) JD20-3 (d) JD27-1

(e) JD27-2 (f) JD27-3

Fig. 11 P-Δ hysteretic loops of specimens

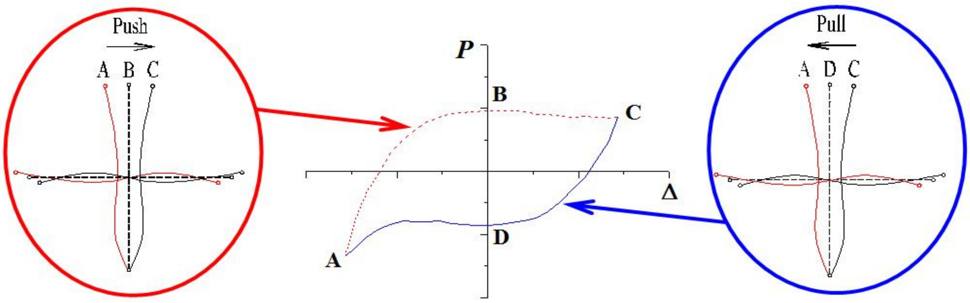

Fig. 12 Loading directions

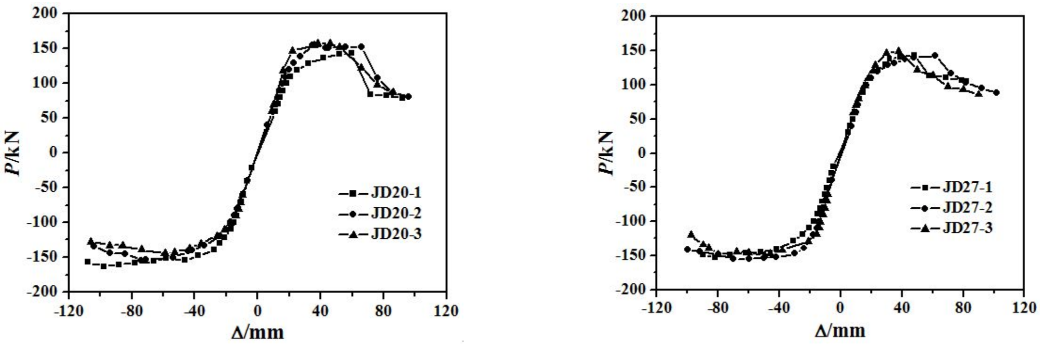

(a) JD20-specimen (b) JD27-specimen

Fig. 13 Comparison of P-Δ skeleton curves of specimens

The skeleton curves of the P-Δ hysteretic loops are shown in Fig. 13. The curves are compared, and it was found that the specimens-JD20 and JD27 have the similar ultimate strength respectively, showing that when the axial compression ratio is less than 0.5, it has no significant impact on the ultimate strength of the abnormal joints. When the axial compression ratio is equal, the ultimate strength of specimen-JD20, of which the section depth ratio of beams is smaller, is slightly higher than that of specimen-JD27. The loads and displacements corresponding to characteristic points of skeleton curves are shown in Table 3. The definition of the yield point was on the basis of the method of universal yield moment (Yao and Chen 2001).

3.3 Mechanical behaviors

Under cyclic loads, the mechanical models of the abnormal joint are shown in Fig. 14. It can be seen that the beam flanges in tension or compression state results from the bending moment at beam end. For the H-shaped beam, the tensile force (or compressive force) of the top flange and the compressive force (or tensile force) of the bottom flange both act at the top panel zone; for the box beam, the compressive force (or tensile force) of the top flange and the tensile force (or compressive force) of the bottom flange act at the top panel zone and the bottom panel zone respectively. Based on the models, the mechanical behaviors of the specimens are discussed as follows:

Table 3 Experimental results under cyclic loading

Specimen	Loading direction	Yield point		Ultimate point	
		P_y*/kN	Δ_y/mm	P_u*/kN	Δ_u/mm
JD20-1	pushed	126.6	29.3	143.6	60.0
	pulled	-141.4	24.1	-162.9	-98.0
JD20-2	pushed	141.3	27.8	154.0	56.0
	pulled	-128.8	-32.2	-154.2	-74.0
JD20-3	pushed	147.9	25.7	157.8	46.0
	pulled	-121.3	-33.8	-144.4	-64.0
JD27-1	pushed	126.9	26.1	142.8	48.0
	pulled	-129.2	-28.9	-152.6	-82.0
JD27-2	pushed	124.7	26.7	142.8	62.0
	pulled	-141.9	-26.3	-154.5	-72.0
JD27-3	pushed	137.8	23.7	149.2	38.0
	pulled	-130.6	-21.2	-150.0	-48.0

* P_y and P_u are the yield strength and ultimate strength under cyclic loading from experimental results, Δ_y and Δ_u are the displacements corresponding to P_y and P_u, respectively

Before the weld between the bottom diaphragm and the column flange cracking, the transfer path of the internal force is clear. The top panel zone and the bottom panel zone bear the load as a whole. Therefore the hysteretic curves (Fig. 11) in corresponding loading cycles are almost symmetrical at the positive and negative directions.

After the weld between the bottom diaphragm and the column flange cracking, the mechanical behaviors of the panel zone are different from the previous behaviors. When the top end of the column is pushed, the tensile force of the box beam bottom flange makes the weld cracks open and propagate (Fig. 15(a)), and doesn't act at the bottom panel zone. The tensile force of the H-shaped beam top flange as well as the compressive force of the H-shaped beam bottom flange and the box beam top flange act at the top panel zone. In this case only the top panel zone bears the load while the bottom panel zone is almost out of work. Because the top panel zone has yielded, the positive loads applied to the specimens change insignificantly in these loading cycles, as shown in Fig. 11. When the top end of the column is pulled, the compressive force of the box beam bottom flange makes the weld cracks close firstly, and the bottom panel zone is still out of work. After the weld cracks are closed (Fig. 15(b)), the compressive force of the box beam bottom flange can act at the bottom panel zone, and the top panel zone and the bottom panel zone can bear the load as a whole. As a result, the negative loads applied to the specimens increased quickly at the later stage of every cycle, as shown in Fig. 11.

3.4 Shear deformation of panel zone

It can be seen from Fig. 14 that the shear force carried by the top panel zone and the bottom panel zone can be expressed as Eqs. (2) and (3) respectively.

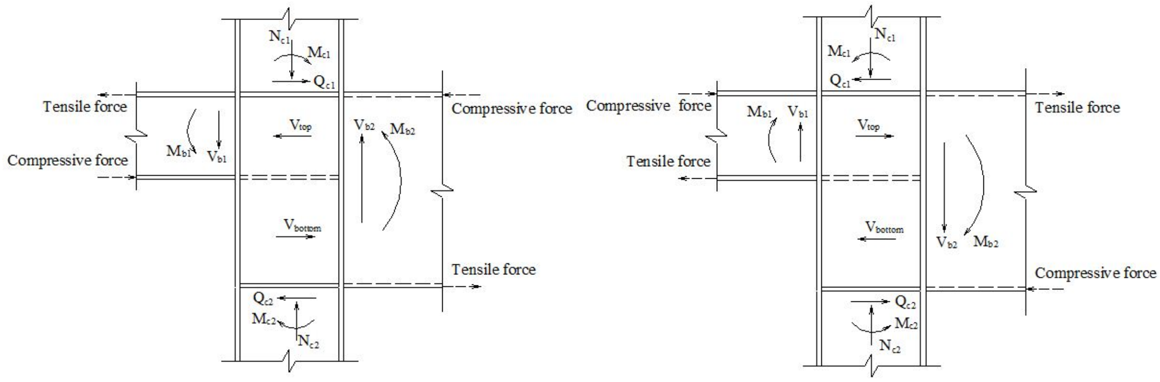

(a) Pushed direction (b) Pulled direction

Fig. 14 Mechanical models

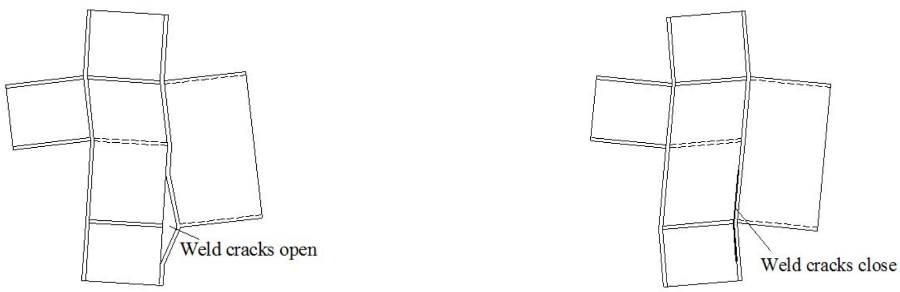

(a) Pushed direction (b) Pulled direction

Fig. 15 Weld cracks open and close

$$V_{\text{top}} = \frac{M_{b1}}{h_{b1}} + \frac{M_{b2}}{h_{b2}} - Q_{c1} \tag{2}$$

$$V_{\text{bottom}} = \frac{M_{b2}}{h_{b2}} - Q_{c2} \tag{3}$$

In which V_{top} and V_{bottom} are the shear force carried by the top panel zone and the bottom panel zone respectively, M_{b1} and M_{b2} are the bending moment carried by the H-shaped beam and the box beam respectively, h_{b1} and h_{b2} are the depths of the H-shaped beam and the box beam respectively, Q_{c1} and Q_{c2} are the shear force carried by the column, $Q_{c1} = Q_{c2}$.

The shear deformation occurs at the panel zone under the shear force. Fig. 16 shows the shear deformation of the panel zone (Ciutina and Dubina 2008). It can be seen that the panel zone changes from rectangle to rhombus periodically under cyclic loads. Through measuring the changing diagonal length of the panel zone, the panel zone rotation, that is the shear deformation of the panel zone, can be calculated according to Eqs. (4)-(7).

$$\overline{X} = \frac{\delta_1 + \delta_1' + \delta_2 + \delta_2'}{2} \tag{4}$$

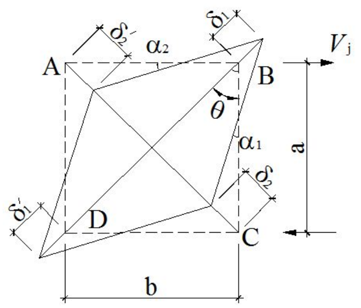

Fig. 16 Shear deformation of the panel zone

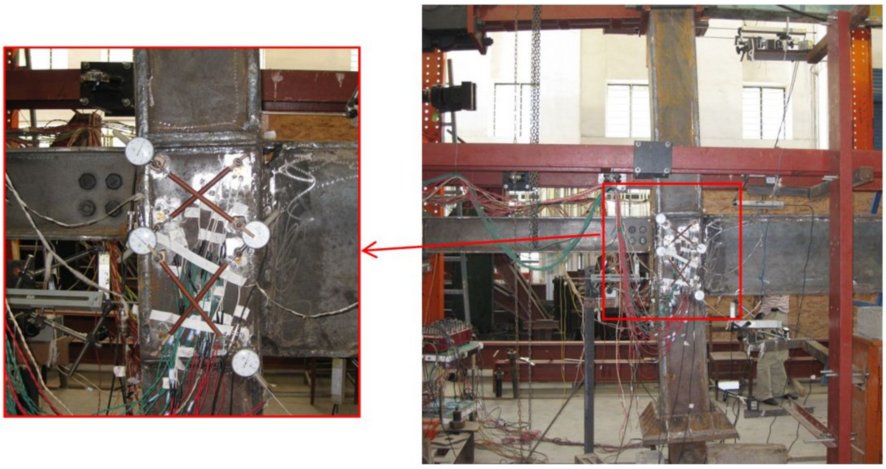

Fig. 17 Patterns about shear deformation of panel zone and global deformation of abnormal joint (JD20-2)

$$\sin\theta = \frac{b}{\sqrt{a^2+b^2}}, \quad \cos\theta = \frac{a}{\sqrt{a^2+b^2}} \tag{5}$$

$$\alpha_1 = \frac{\sin\theta \cdot \overline{X}}{a}, \quad \alpha_2 = \frac{\cos\theta \cdot \overline{X}}{b} \tag{6}$$

$$\gamma = \alpha_1 + \alpha_2 = \frac{\sin\theta \cdot \overline{X}}{a} + \frac{\cos\theta \cdot \overline{X}}{b} = \frac{\sqrt{a^2+b^2}}{ab}\overline{X} \tag{7}$$

In which γ is the panel zone rotation, $(\delta_1 + \delta'_1)$ and $(\delta_2 + \delta'_2)$ are the relative displacements (in absolute value) recorded by dial gauges, a and b are the vertical and horizontal dimensions between the measuring points.

The pattern about shear deformations of the panel zone as well as global deformations of the abnormal joint at the last loading cycle is shown in Fig. 17. Based on the experimental results, the relationship between the shear deformation and the shear force of the panel zone is obtained, as shown in Fig. 18. Observations can be made as follows:

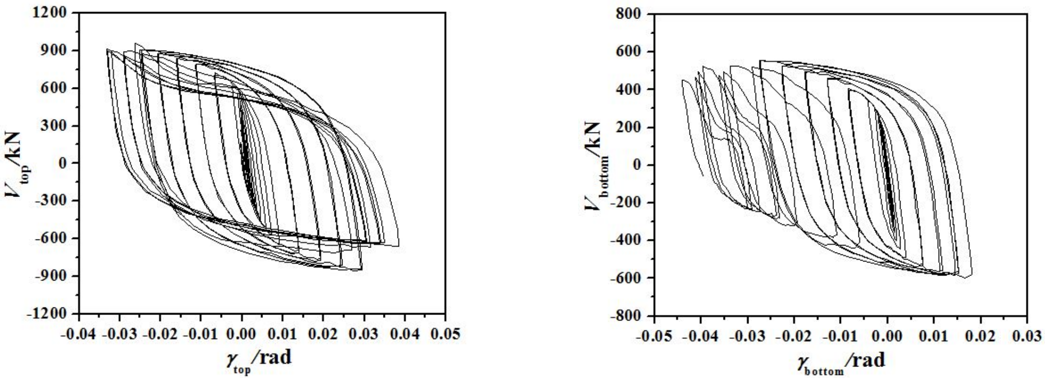

(a) Top panel zone (b) Bottom panel zone

Fig. 18 Hysteretic loops of rotation and shear force of the panel zone (JD20-2)

- The shear deformation of the top panel zone increased continuously at both loading directions, and the maximum of rotation could reach to 0.04 rad, showing good deformation capacity. Before the weld between the bottom diaphragm and the column flange cracking, the rotation of the bottom panel zone increased regularly and the synchronous deformation was about 0.01 rad smaller than that of the top panel zone. After the weld cracking, however, the deformation increased in one direction only. It can be seen that the top panel zone and the bottom panel zone don't work as a whole, although they are both the panel zone.
- The changing tendency of the shear force carried by the top panel zone and the bottom panel zone is similar to that of the load applied to the specimens, which is mainly affected by mechanical behaviors.

3.5 Shear strength calculation of panel zone

Comparing Eq. (2) with Eq. (3), it can be seen that the shear force carried by the top panel zone is much lager than that by the bottom panel zone, which can be confirmed through the experimental results (Fig. 16). So the shear strength of the abnormal joint panel zone depends on the top panel zone.

AISC (2005) specifies that the shear strength of the normal joint panel zone can be calculated by the following equation

$$V_u = 0.6 f_y d_c t_w \left(1 + \frac{3 b_{cf} t_{cf}^2}{d_b d_c t_w} \right) \tag{8}$$

In which f_y is the yield strength of material, d_c is the depth of the column, t_w is the web thickness of the panel zone, b_{cf} is the width of the column flange, t_{cf} is the thickness of the column flange, d_b is the depth of the beam.

The second term in the bracket accounts for the contribution of the column flanges (Sherif 2000). Plugging the corresponding data into Eqs. (2) and (8) respectively, the maximum value of the shear force carried by the top panel zone ($V_{\mathrm{top}}^{\max}$) in the test and the shear strength of the top panel zone (V_{top}^{u}) according to the calculated method of normal joint can be obtained, as shown in

Table 4. The ratio of $V_{\mathrm{top}}^{\max}$ and V_{top}^{u} is also listed in the Table. It can be seen that $V_{\mathrm{top}}^{\max}$ is much larger than V_{top}^{u}, which indicating that the shear strength of the abnormal joint panel zone is larger than that of the normal joint panel zone with the same condition, and the equation for shear strength of the normal joint panel zone, provided by AISC specification, is no longer applicable to the abnormal joint. It can be explained as the result of the restriction of the bottom panel zone to the top panel zone. In the loading process, the top panel zone yields firstly. At this time, the bottom panel zone doesn't yield, and it can still bear the load and the shear deformation is small. So the bottom panel zone can restrict the shear deformation of the top panel zone, which makes the shear force carried by the top panel zone increase continuously. When the bottom panel zone yields completely, the shear force carried by the top panel zone can reach the maximum.

Comparing between the ratio of $V_{\mathrm{top}}^{\max}$ and V_{top}^{u}, it can be found that the values of specimen-JD20 are larger than those of specimen-JD27, which shows that the restriction of the bottom panel zone to the top panel zone of specimen-JD20 is stronger than that of specimen-JD27. So it can be concluded that the restriction becomes stronger with the decrease of the section depth ratio of beams.

Based on the equation for the shear strength of the normal joint panel zone given by AISC specification and taking the restriction of the bottom panel zone into consideration, the proposed equation for the shear strength of the abnormal joint panel zone is established as

$$V_u = 0.6 f_y d_c t_w \left[1 + \frac{3 b_{cf} t_{cf}^2}{d_{b1} d_c t_w} + \alpha(1-\beta) \right] \tag{9}$$

In which α is the influence coefficient considering the restriction of the bottom panel zone to the top panel zone, the implication of other symbols is the same as those in Eqs. (1) and (8).

α is an undetermined coefficient and can be worked out inversely according to Eq. (9) and the experimental results, as shown in Fig. 19 and Table 5.

Based on Table 5, α can be approximately determined as 1, and then Eq. (9) can be expressed as

$$V_u = 0.6 f_y d_c t_w \left(2 + \frac{3 b_{cf} t_{cf}^2}{d_{b1} d_c t_w} - \beta \right) \tag{10}$$

Eq. (10) is the equation for the shear strength of the abnormal joint panel zone, and is available for the design of beam-to-column abnormal joint in the steel moment-resisting frame. However, it should be noted that the equation is only suitable for the abnormal joint of the H-shaped or box column and beams with different depths, and the axial compression ratio should be less than 0.5. In addition, β should be limited, because if the value is too small, the height of the bottom panel

Table 4 Calculated results of the top panel zone

Specimen	JD20-1	JD20-2	JD20-3	JD27-1	JD27-2	JD27-3
$V_{\mathrm{top}}^{\max}$ (kN)	965.7	960.5	1006.0	862.1	877.7	805.5
V_{top}^{u} (kN)	659.5	659.5	659.5	633.4	633.4	633.4
$V_{\mathrm{top}}^{\max} / V_{\mathrm{top}}^{u}$	1.464	1.456	1.525	1.361	1.386	1.272

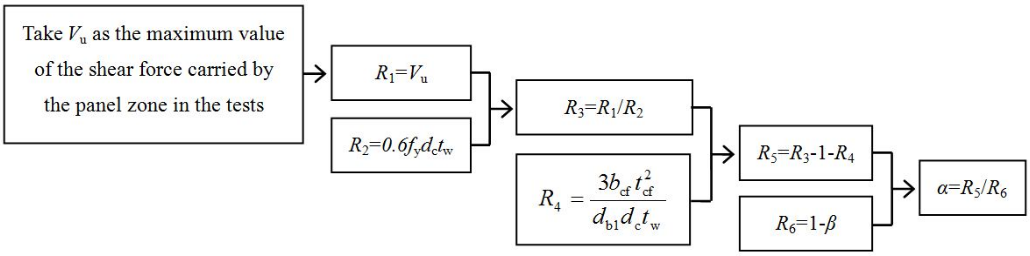

Fig. 19 Flow chart for determination of coefficient α

Table 5 Determination of coefficient α

Specimen	R_1	R_2	R_3	R_4	R_5	R_6	α	Average of α
JD20-1	965.7	558.9	1.728	0.180	0.548	0.56	0.979	0.990
JD20-2	960.5	558.9	1.719	0.180	0.543	0.56	0.970	
JD20-3	1006.0	558.9	1.800	0.180	0.620	0.56	1.107	
JD27-1	862.1	558.9	1.542	0.133	0.409	0.40	1.023	
JD27-2	877.7	558.9	1.570	0.133	0.437	0.40	1.093	
JD27-3	805.5	558.9	1.441	0.133	0.308	0.40	0.770	

zone is large, and its restriction to the top panel zone may not be proportional to $(1-\beta)$; if the value is too large, the height of the bottom panel zone is small, and its restriction is small, even can be ignored. Therefore, based on the test, the suggested range of β is $0.4 \le \beta \le 0.8$. Take β as 0.4, if $\beta < 0.4$; take β as 0.8, if $\beta > 0.8$.

4. Conclusions

The purpose of this investigation was to study the cyclic behavior of the abnormal joint of box column with H-shaped beam and box beam. Based on the experimental results described in this paper, the following conclusions can be drawn:

- For all the specimens, the first signs of yielding occurred at the center of the top panel zone. After the panel zone yielding completely, there were four types of failure patterns occurring in sequence during the following loading process. There was almost no yield at the end of the beams and the columns until the tests terminated.
- The P-Δ hysteretic loops are in a shuttle shape, but the curves at the pushed and pulled directions have different changing tendency in the later of loading process, which is closely related to the mechanical behaviors.
- When the axial compression ratio is less than 0.5, there is no significant impact on the ultimate strength of the specimens. With the decrease of the section depth ratio of beams, the ultimate strength tends to increase.
- The mechanical behaviors of the specimens were impacted greatly by the crack of weld between the bottom diaphragm and the column flange as well as its propagation. When the crack is open, the internal force of the box beam bottom flange can’t act at the bottom panel

zone, and only the top panel zone bears the load; when the crack is closed, the internal force of the box bottom flange can act at the bottom panel zone, and the top panel zone and the bottom panel zone can bear the load as a whole.

- The top panel zone has good deformation capacity, and the maximum rotation can reach to 0.04rad. The rotation of the bottom panel zone is smaller than that of the top panel zone. The top panel zone and the bottom panel zone don't work as a whole.
- The bottom panel zone can restrict the shear deformation of the top panel zone, resulting in that the shear strength of the abnormal joint panel zone is larger than that of the normal joint panel zone. So the equation for the shear strength of the normal joint panel zone, provided by AISC specification, is no longer applicable to the abnormal joint, and a new equation for the shear strength of the abnormal joint panel zone is proposed.

Acknowledgments

The authors would like to thank the financial support provided by Natural Science Foundation of China (Granted No. 51308444), Postdoctoral Science Foundation of China (Granted No. 20080440814), Natural Science Basic Research Foundation of Shaanxi Province (Granted No. 2014JQ7288) and Program for Innovation Team of Education Ministry of China (Granted No. IRT13089), Shanxi Province (Granted No. 2014KCT-31) and Xi'an University of Architecture and Technology.

References

AISC (2005), Load and resistance factor design specification for structural steel buildings; American Institute of Steel Construction, Chicago, IL, America.

Ciutina, A.L. and Dubina, D. (2008), "Column web stiffening of steel beam-to-column joints subjected to seismic actions", *J. Struct. Eng.*, **134**(3), 505-510.

He, J., Yoda, T., Takaky, H., Liu, Y.Q., Chen, A.R. and Iura, M. (2010), "Experimental and numerical study on cyclic behavior of steel beam-to-column Joints", *Int. J. Steel Struct.*, **10**(2), 131-146.

Imai, K., Yoshida, Y., Saijo, M., Watanabe, T. and Hirano, M. (1991), "An experimental report on elasto-plastics behaviors of beam-to-column connections with an offset in right and left beam positions", *J. Struct. Construct. Eng.*, **425**, 27-35.

JGJ101-96 (1997), *Specification of Test Methods for Earthquake Resistant Building*, Beijing, China.

Kuwahara, S., Kumano, M. and Inoue, M. (2000), "The elasto-plastic behaviors of joint panels at the connection of rectangular steel column and two H-shaped beams with different depth", *J. Struct. Construct. Eng.*, **533**, 175-181.

Lee, K.M., Li, R., Jung, H.T., Chen, L.Y. and Oh, K.W. (2013), "Cyclic testing of weak-axis steel moment connections", *Steel Compos. Struct.*, *Int. J.*, **15**(5), 507-518.

Li, C. and Chen, Y.Y. (2009), "Development of research on shear bearing capacity of joint between circular tubular column and beam of steel frame", *Progress in Steel Building Structures*, **11**(6), 33-39.

Loulelis, D., Hatzigeorgiou, G.D. and Beskos, D.E. (2012), "Moment resisting steel frames under repeated earthquakes", *Earthq. Struct.*, *Int. J.*, **3**(3), 231-248.

Peng, X.N., Xue, J.Y., Liu, Z.Q. and Hu, Z.B. (2010), "Mechanical behaviors and design method for irregular joints in rigid steel frames", *J. Civil*, *Architect. Environ. Eng.*, **32**(3), 22-26.

Sherif, E.T. (2000), "Panel zone yielding in steel moment connection", *Eng. J.*, **37**, 120-130.

Sui, W.N., Sun, X., Wang, Z.F. and Li, G.C. (2013), "Research on design method and mechanical performance of the irregular joint with different beam depths", *Eng. Mech.*, **30**(Supp1), 83-88.

Yang, C.M. and Kim, Y.M. (2007), "Cyclic behavior of bolted and welded beam-to-column joints", *Int*. *J*. *Mech*. *Sci*., **49**, 635-649.
Yao, Q.F. and Chen, P. (2001), *Civil Engineering Structure Test*, China Architecture & Building Press, Beijing, China.

CC